Available online at www.sciencedirect.com

SCIENCE DIRECT®

International Journal of Solids and Structures 41 (2004) 5979–5993

INTERNATIONAL JOURNAL OF SOLIDS and STRUCTURES

www.elsevier.com/locate/ijsolstr

Formation of adiabatic shear band in metal matrix composites

L.H. Dai *, L.F. Liu, Y.L. Bai

State Key Laboratory of Nonlinear Mechanics (LNM), Institute of Mechanics, Chinese Academy of Sciences, Beijing 100080, PR China

Received 10 May 2004
Available online 20 June 2004

Abstract

A modified single-pulse loading split Hopkinson torsion bar (SSHTB) is introduced to investigate adiabatic shear banding behavior in SiCp particle reinforced 2024 Al composites in this work. The experimental results showed that formation of adiabatic shear band in the composite with smaller particles is more readily observed than that in the composite with larger particles. To characterize this size-dependent deformation localization behavior of particle reinforced metal matrix composites (MMCp), a strain gradient dependent shear instability analysis was performed. The result demonstrated that high strain gradient provides a deriving force for the formation of adiabatic shear banding in MMCp.

1. Introduction

Narrow bands of intense shear deformation are commonly observed during high strain rate plastic deformation of various materials, such as metals, polymers and geological materials, in such situations as impact of projectiles and vehicles, high speed materials processing and forming. These bands are known as adiabatic shear bands. Under favorable conditions, the formation of adiabatic shear bands is often followed by ductile fracture. Hence, an in-depth understanding of the mechanisms leading to the formation and development of adiabatic shear localization is of great practical interest.

Early observations of adiabatic shear bands can be traced back to Henri Tresca (1878) and Harold Massey (1921) who described them as "adiabatic heat lines". Later, the adiabatic shear banding phenomenon was dramatically demonstrated by Zener and Hollomon (1944) who noted that an increase of the strain rate tends to change the deformation conditions from isothermal to adiabatic and macroscopically homogeneous plastic deformation becomes unstable if the slope of the adiabatic stress-strain curve becomes negative. Since then, extensive research efforts have been made to understand adiabatic shear banding, see e.g, some review papers and monographs (Rogers, 1979; Shawki and Clifton, 1989; Bai and Dodd, 1992; Meyers, 1994; Ramesh, 1994; Meyer et al., 1994; El-Magd, 1997; Perzyna, 1998; Wright, 2002). It is well

* Corresponding author. Tel.: +86-10-6261-6852; fax: +86-10-6256-1284.
E-mail address: lhdai@lnm.imech.ac.cn (L.H. Dai).

0020-7683/$ - see front matter © 2004 Elsevier Ltd. All rights reserved.
doi:10.1016/j.ijsolstr.2004.05.023

recognized that the primary mechanism for the formation of adiabatic shear localization is the thermomechanical mechanism. Due to interactions of microstructures of materials, the initial uniform plastic deformation may become inhomogeneous. At high loading rates, the lack of time for global heat conduction combined with inhomogeneous plastic deformation will induce inhomogeneous heating which in turn leads to local material softening and additional plastic deformation so that localized shear bands are finally formed. Also, recent research works from Meyers and co-workers (Meyers et al., 2001; Xue et al., 2002) have demonstrated that adiabatic shear bands often exhibit a self-organization pattern.

A number of authors have attempted to determine the critical conditions for the onset of adiabatic shear banding. Since analytical solutions for initial boundary-value problems of dynamic simple shear are available only for a limited number of special deformations and constitutive relations, the linear stability analysis has been a useful tool for examining sufficient conditions and/or necessary conditions for adiabatic shear instability. Clifton (1980, 1984) and Bai (1981, 1982) have proposed instability criteria derived from one-dimensional linear stability analyses for simple shear plastic flow. Burns (1985) used a two-timing asymptotic expansion, for a particular constitutive model, to include the time dependence of homogeneous solution in the stability analyses. Anand et al. (1987) have presented a three-dimensional generation of the linear perturbation analysis for the onset of shear localization. Molinari and Clifton (1987) and Shawki (1992) obtained the critical conditions of adiabatic shear band formation for some particular cases by using the non-linear stability analysis approach. Fressengeas and Molinari (1987) introduced a relative perturbation method for adiabatic shear instability. In a series of works, Wright and co-workers (Wright and Ockendon, 1996; Wright, 2003; Schoenfeld and Wright, 2003) developed scaling laws for adiabatic shear banding.

Although the extensive research activities and a great progress in understanding adiabatic shear banding have been made during the past several decades, it is noted that the great majority of the aforementioned efforts were focused on monolithic materials. However, relatively limited works have been made to address adiabatic shear banding in metal matrix composites (Lee et al., 1993; Dai et al., 2000). It is well known that the microstructures of materials have a significant influence on the onset and evolution of adiabatic shear band. This is especially true for composite materials. The different combinations of thermomechanical properties constitute an environment for thermomechanical coupling between the phases and provide a driving force for inhomogeneous deformation. For particle reinforced metal matrix composites (MMCp), recent experimental investigations have demonstrated that the formation of adiabatic shear band exhibit a strong size-dependent behavior. By making use of the split Hopkinson pressure bar (SHPB), Ling et al. (1994, 2000) performed a series of impact compressive tests for 2124 aluminum matrix composites reinforced with three sizes of SiC particles. Their experimental results have shown that the formation of adiabatic shear bands in the composite reinforced with smaller particles is more readily observed than that in the composite with larger particles for a fixed particle volume fraction. Furthermore, significant inhomogeneous plastic deformation patterns and steep plastic strain gradients across the localized zones in the matrix were observed. This size-dependent adiabatic shear banding phenomenon was also demonstrated by Zhou (1998a,b) in his numerical investigations on adiabatic shear banding in tungsten composites. All these have naturally raised the following questions: what are the physical origin and mechanisms of this size-dependent adiabatic shear banding behavior in MMCp? What is the role of the particle size or the strain gradient in the formation of adiabatic shear banding in MMCp? Obviously, the previously developed adiabatic shear banding theories that are based on the classical constitutive relations containing no internal length scales, cannot answer these questions.

To address the size-dependent adiabatic shear banding behavior, the strain gradient term is required to be incorporated into the conventional constitutive equation. Motivated by this point, Aifantis (1984, 1992, 1999), Zbib and Aifantis (1992), Zhu et al. (1995), and Sluys et al. (1993, 2000) developed some phenomenological strain gradient plasticity theories by incorporating higher strain gradients (the terms of Laplacian strain terms) into the flow stress or the yield function to examine the effect of the strain gradient

on shear banding. Moreover, Batra (1987, 1990, 1999) generalized Green et al.'s (1968) work for dipolar elastic–plastic materials to simple shear deformations of dipolar thermoviscoplastic materials to investigate the strain gradient effect on the onset of shear bands. It is noted that the aforementioned investigations were concentrated on monolithic materials. However, how to understand the effect of the strain gradient or the reinforcing particle size on adiabatic shear banding in two-phase MMCp is still remained.

The objective of this paper is to elucidate the effect of the reinforcing particle size or the strain gradient on the onset of adiabatic shear banding in particle reinforced metal matrix composites (MMCp). To this end, the formation of adiabatic shear band in 2024 aluminum matrix composites reinforced with 15% volume fraction of 3.5, 10, and 20 μm SiC particles, respectively, is investigated by using single-pulse split Hopkinson torsion bar (SSHTB). To understand the experimentally observed size-dependent adiabatic shear banding behavior, the linear stability analysis is made by making use of the strain gradient dependent constitutive equation which was recently developed by Liu et al. (2003). From these experimental and theoretical investigations, the effect of the reinforcing particle size or the strain gradient on the formation of adiabatic shear banding in MMCp is revealed.

2. Experimental approach

2.1. Materials description and specimen preparation

The materials used in this study were 2024 aluminum alloy reinforced with 15% volume fraction of 3.5, 10, and 20 μm SiC particles respectively, which were processed by the powder metallurgy method. These materials were in the form of cylindrical bar with a diameter of 20 mm. Before testing, the composites were solution heat treated, i.e., heated up to 530 °C and kept this constant temperature for 55 min, then quenched in cold water. Then, the materials were machined into thin-walled tubular specimens for dynamic torsional testing.

2.2. Dynamic torsional shear tests

Because of the remarkable advantages of the split Hopkinson torsion bar (SHTB), such as the simple stress state within a specimen, no wave dispersion and friction, this technique is the most widely used to investigate adiabatic shear banding in various materials. For adiabatic shear band study, a critical need is to reveal how the microstructure of materials evolves during the shear banding process and how this microstructure evolution affects the macroscopic response of materials. However, the standard SHTB cannot provide required quantitative post-mortem observation of the deformed microstructure due to its loading wave reverberation. The stress wave reverberation resulting from the reflection of the loading wave in the bar system imposes multiple loadings on the specimen and destroys the real deformed microstructure after the first loading pulse. In order to solve this problem, a standard SHTB was modified in our laboratory by Xue et al. (1995a,b) to eliminate the effect of loading reverberation. The main modification involves two unloading bars attached to the two ends of the original main bar system, a new loading head and a couple of specially designed clutches. Thus, the secondary loading waves were wholly trapped in the two unloading bars and a complete single-pulse is introduced in the new bar system. In comparison with the standard SHTB, we call the modified bar system as a single-pulse split Hopkinson torsion bar (SSHTB).

For our present study, the SSHTB was used to investigate the effect of particle size on the formation of adiabatic shear banding in SiCp/2024 Al matrix composites. The schematic diagram of the SSHTB is shown in Fig. 1. Before testing, calibration was carried out to examine the ability of SSHTB to eliminate wave reverberation. The calibrating stress wave profiles on the standard SHTB and SSHTB are shown in Figs. 2 and 3, respectively. From Fig. 3, one can clearly see that only a single stress pulse is introduced in SSHTB.

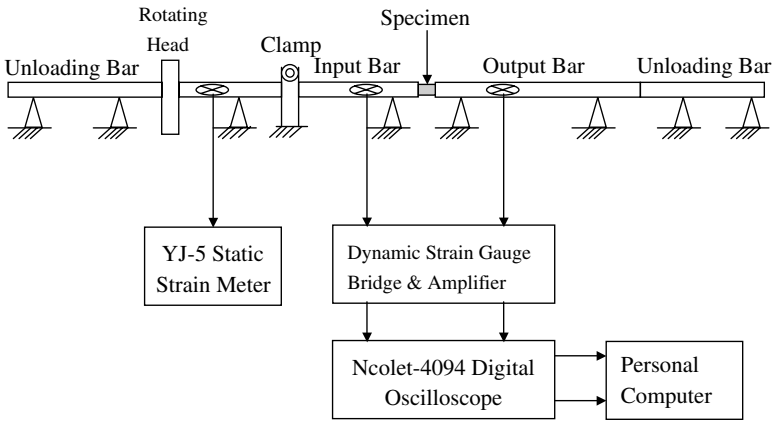

Fig. 1. Schematic diagram of the single-pulse Hopkinson torsion bar (SSHTB).

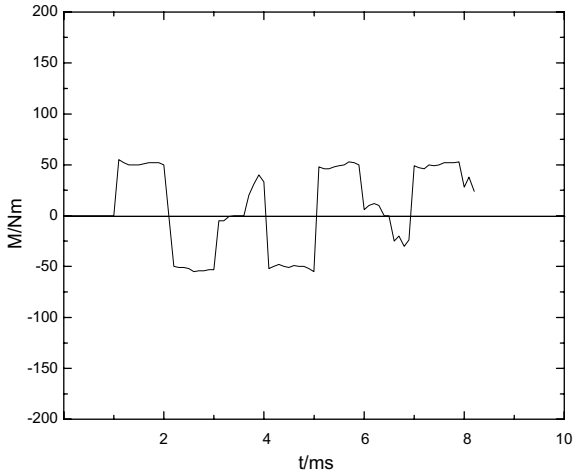

Fig. 2. A calibrating oscillogram of a standard split Hopkinson torsion bar (SHTB).

In the experiment, the short thin-walled tubular specimen, as shown in Fig. 4, was sandwiched between the input and output bars, 25 mm in diameter. At first, a hydraulic pump was actuated to twist the front portion of the input bar in order to store torsional energy between the rotating head and the clamp. The twisting torque was monitored by a static shear strain gauge as shown in Fig. 1. As the clamp is abruptly released, a torsional impulse propagates through the input bar and loads the specimen. At the interface, a part of the torsional wave is reflected back to the input bar and the other part is transmitted into the output bar. According to the elastic properties of the bars and the recorded wave profiles, the dynamic shear stress–strain in the specimen can be measured.

The incident, reflected and transmitted pulses were measured by two sets of 90° rosette strain gauges mounted on the input and output bars, respectively. Signals from the input and output bars were conditioned by dynamic strain amplifiers, and a digital oscilloscope was used for data acquisition. Therefore, the average shear stress, strain, and shear strain rate can be calculated according to the wave forms of

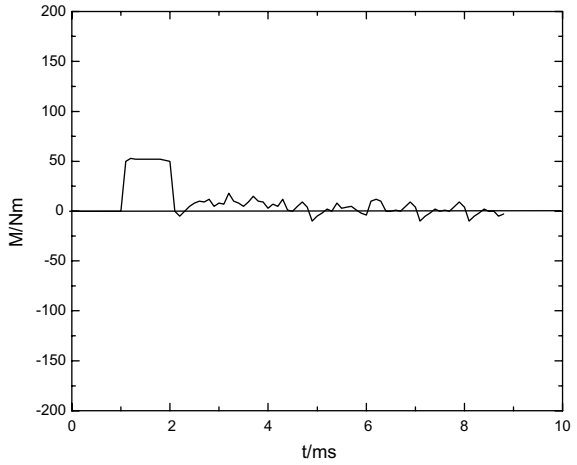

Fig. 3. A calibrating oscillogram of single-pulse split Hopkinson torsion bar (SSHTB).

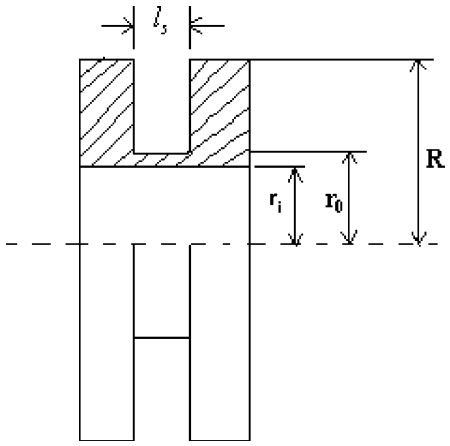

Fig. 4. Schematic description of the thin-walled tubular specimen.

the incident torque, $M_i(t)$, and the reflected torque, $M_r(t)$ measured by the gauges on the input bar and the transmitted torque, $M_t(t)$ measured by gauges on the output bar as follows:

$$\tau = \frac{M_t(t)}{2\pi r_s^2 \delta} \tag{1}$$

$$\dot{\gamma} = \frac{2r_s C_0}{l_s J_b G_b}\left(M_i(t) - M_t(t)\right) \tag{2}$$

$$\gamma = \frac{2r_s C_0}{l_s J_b G_b}\int_0^t \left(M_i(t) - M_t(t)\right)\mathrm{d}t \tag{3}$$

where l_s, r_s, δ are the gauge length, mean radius, and thickness of the specimen, respectively. In addition, C_0, J_b, G_b are elastic wave speed, the polar moment of inertia, and the shear modulus of the bars, respectively.

In the present work, a series of tests were performed on the SSHTB system under the same loading duration and strain rate. The duration of the incident wave pulse was kept about 600 μs. The dynamic strain rate was fixed at $\sim$1000 s^{-1}. After testing, samples were cut for microscopic observations.

2.3. Experimental results

Dynamic shear stress-strain curves of both SiCpP/2024Al matrix composites and unreinforced 2024 Al alloy are shown in Fig. 5. One of the prominent features in these curves is that, the shear flow stress of the composites exhibits a size-dependent behavior. The smaller the SiCp particles are, the higher the shear flow stresses of composites are. Among them, the composite containing 3.5 μm SiCp particles is of the highest shear flow stress and the matrix material, 2024 Al alloy, is of the lowest shear flow stress under the same loading condition. Furthermore, one can find from Fig. 5, the maximum shear strain for the composite with 3.5 μm SiCp particles is about 0.4, over which the stress–strain curve drops down and the specimen seems to undergo failure. But at this shear strain, specimens of other three kinds of materials do not show any evidence of macroscopic failure according to the stress–strain curves. This phenomenon demonstrates that the small SiCp has not only increased the stress but also decreased the ductility of the composites. The observation is only one aspect of the problem, from the microscopic observations of deformed samples we found another aspect of the problem.

To investigate the formation of adiabatic shear band, we marked some well-proportioned lines on the inner walls of the specimens before testing. After tests, the outside walls of the thin-walled tube specimens were cut according to the distortion of the marked lines, and then finely polished and eroded to form observable planes for microscopic examinations. Corrosive solution is 2.5%HNO_3+1.5%HCl + 1%HF+95%H_2O. A close-up observation of loaded samples was carried out using NEOPHOT-21 optical microscope. The typical microscopic pictures are shown in Fig. 6. The micrographs demonstrate that under the identical loading condition, the incorporation of reinforcing particles could block the deformation of matrix. Furthermore, one

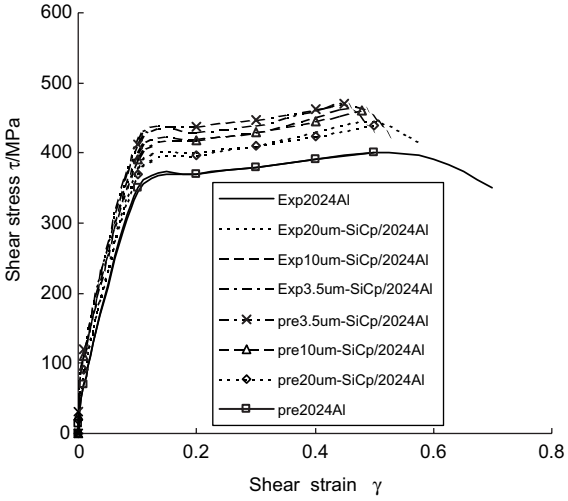

Fig. 5. A comparison of predicted shear stress strain curves with the experimental results for SiCp/2024 Al matrix composites under a strain rate of 1000 s^{-1}.

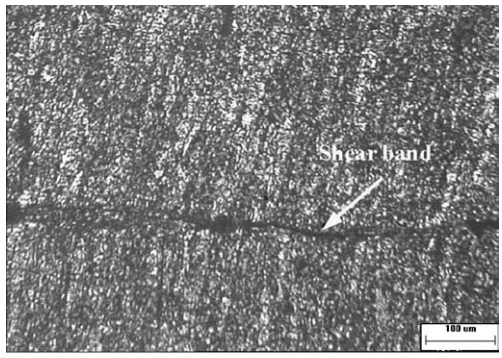

(a) $d_p = 3.5\mu m$

(b) $d_p = 10\mu m$

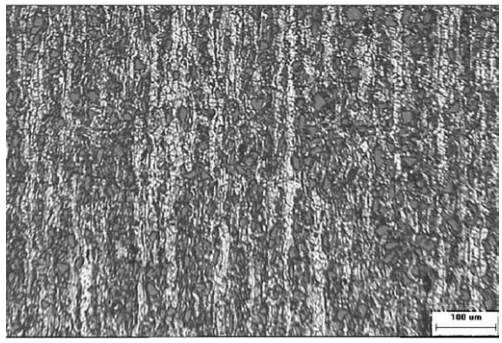

(c) $d_p = 20\mu m$

Fig. 6. Micrographs of deformation patterns in SiCp/2024 Al composites: (a) 3.5 μm SiC particle; (b) 10 μm SiC particle and (c) 20 μm SiC particle.

can find from the micrographs that the formation of adiabatic shear band in SiCp/2024Al matrix composites depends strongly on the reinforcing particle size. Fig. 6a is a microscopic picture of the composite reinforced with 3.5 μm SiC particles. From the picture, large plastic flow was localized in a very limited region and shear band was obviously formed. In the shear band, a part of aligned particles has oriented along the large flow direction. However, under the same magnification, the microscopic deformations in the other two composites

containing SiCp particles of 10 μm and 20 μm do not show obvious localized shear bands, as shown in Fig. 6b and c, respectively. In the composites containing SiCp particles of 10 μm, several small plastic flow regions and localized flow trends were observed, but shear band was not formed finally. In the composites containing SiCp particles of 20 μm, neither localized plastic flow trends nor shear bands were observed. Recent experimental investigation from Ling et al. (1994, 2000) on SiCp/2124Al composites and the numerical simulations form Zhou (1998a,b) on tungsten composites have also demonstrated that adiabatic shear bands can readily be observed in a composite reinforced with smaller particles.

For MMCp, the incorporation of reinforcing ceramic particles (e.g. SiC particles) into the metal matrix will induce an inhomogeneous plastic deformation in the matrix and this inhomogeneous deformation can be characterized by plastic strain gradient. Our previous attempts have demonstrated that the smaller the particle size, the higher the strain gradient. The size effect of MMCp can thus be characterized by the strain gradient effect (Dai et al., 1999, 2001; Liu et al., 2003). According to this understanding, the aforementioned experimental observation implies that the small reinforcing particles act as a deformation localization stimulator, and a high strain gradient is a strong driving force for the onset of adiabatic shear banding in MMCp. In next section, a linear stability analysis will be made to investigate the effect of the strain gradient on the onset of adiabatic shear banding in MMCp. The role of the strain gradient in the strengthening behavior of MMCp have been discussed before (Dai et al., 1999, 2001; Liu et al., 2003).

3. Linear stability analysis and discussions

3.1. Governing equations

It is noted that a strain gradient term is required to be incorporated into the equation of the flow stress for characterizing the size-dependent adiabatic shear banding behavior of MMCp. Assume the strengthening for MMCp is mainly attributed to the deformation resistance induced by the reinforcing particles. According to Taylor's dislocation strengthening relation and the geometrically necessary dislocation concept (Ashby, 1970; Meyers and Chawla, 1983), a strain gradient dependent constitutive equation for two-phase MMCp was developed by Dai et al. (1999) and Liu et al. (2003). The form of this strain gradient dependent constitutive equation is written as

$$\sigma_{\mathrm{c}} = \sigma_{\mathrm{m}}(1 + \hat{l}\eta)^{v} \tag{4}$$

where σ_{m} and σ_{c} are the flow stresses of the matrix and MMCp, respectively, v is a dimensionless constant, and $\hat{l} = 3a^2 b(\mu_{\mathrm{m}}/\sigma_{\mathrm{m}})^2$ is a material length, a is dimensionless parameter, b Burgers vector, μ_{m} is the shear modulus of the matrix material. While η is the effective strain gradient and its general expression is given by (Fleck and Hutchinson, 1997; Gao et al., 1999a)

$$\eta = \sqrt{c_1\eta_{iik}\eta_{jjk} + c_2\eta_{ijk}\eta_{ijk} + c_3\eta_{ijk}\eta_{kji}} \tag{5}$$

where the three effective strain gradient constants (c_1, c_2, c_3) scale the three quadratic invariants for the incompressible third rank strain gradient tensor η_{ijk}. From continuum plasticity point of view, the effective strain gradient η measures the density of geometrically necessary dislocations that are required for compatible deformation of various parts in materials (Gao et al., 1999b). For MMCp, these three constants were determined by three dislocation models consisting of pure torsion, plain strain bending, and two-dimensional axisymmetric cell and given by (Liu et al., 2003)

$$
\begin{aligned}
c_1 &= \frac{1}{4}\left(1+\frac{2lf_p}{d_p}\right)^2 - \frac{1}{6}\left(1+\frac{4lf_p}{d_p}\right)^2 - \frac{1}{12} \\
c_2 &= \frac{1}{6}\left(1+\frac{4lf_p}{d_p}\right)^2 + \frac{1}{12} \\
c_3 &= -\frac{1}{6}\left(1+\frac{4lf_p}{d_p}\right)^2 + \frac{1}{6},
\end{aligned}
\tag{6}
$$

where f_p and d_p are the volume faction and diameter of particles respectively, and l is a geometrical factor of unit order with length scale. One can see clearly from Eqs. (5) and (6) that both the size and the volume fraction of the reinforcing particles exert an influence on the strain gradient, and the smaller the particle size (particle diameter d_p) is, the higher the strain gradient is. If $f_p = 0$, the result given by Eq. (6) is turned back to that of monolithic materials case (Fleck and Hutchinson, 1997; Gao et al., 1999), i.e., $c_1 = c_3 = 0$, $c_2 = \frac{1}{4}$. It is noted that if the *strain gradient independent* flow stress of the matrix (σ_m) is known, the *strain gradient-dependent* flow stress of two-phase MMCp (σ_c) can readily be obtained from Eq. (4). It is seen from Eqs. (4)–(6) that the strengthening effect due to introducing the particles into the metal matrix can be characterized by (σ_c/σ_m), which is controlled by the strain gradient η and the characteristic microstructural length $\hat{l}$. Furthermore, for MMCp with a fixed volume fraction of reinforcing particles, one can find that the smaller the particle size is, the higher the strain gradient is and the higher the strengthening effect is.

For uniaxial compression case, the utility of Eqs. (4)–(6) was verified in our previous study (Liu et al., 2003) by comparing the predicted stress–strain curves with the uniaxial-compression experimental results for SiCp/2124Al and SiCp/A356 Al matrix composites. For the present torsional shear case, the comparison of the predicted stress–strain curves obtained using the constitutive equations (4)–(6) and (20) with the experimental results for SiCp/2024 Al matrix composites is shown in Fig. 5. From this figure, one can find that the predicted results are slightly lower than those of the experimental results. However, the relative errors at all strain graining points were less than 10%. These relatively low predicted values may be due to the fact that some other secondary contributions to the strengthening, namely, the strain rate dependent size effect, the thermal mismatch between particles and the matrix, are not incorporated into the model. In spite of this, it is seen from the comparison that the predicted results are in agreement with the experimental data quite well.

Now, we consider the dynamic thermomechanical deformation of a strain gradient-dependent thermovicoplastic two-phase MMCp under the following one-dimensional simple shearing:

$$
\left.
\begin{aligned}
x &= u(x,y) + X \\
y &= Y \\
z &= Z
\end{aligned}
\right\}
\tag{7}
$$

where u is displacement, x, y, z are Eulerian and X, Y, Z are the Lagrangian coordinates. The governing equations for the present problem can be written as

$$\tau = f(\theta, \gamma, \dot{\gamma}, \eta) \tag{8}$$

$$\frac{\partial^2 \tau}{\partial y^2} = \rho \frac{\partial^2 \gamma}{\partial t^2} \tag{9}$$

$$K\tau \frac{\partial \gamma}{\partial t} = \rho c_v \frac{\partial \theta}{\partial t} - \lambda \frac{\partial^2 \theta}{\partial y^2} \tag{10}$$

where Eq. (8) is the strain gradient dependent constitutive equation of MMCp, Eq. (9) is the motion equation, Eq. (10) is the energy equation; with ρ is density, c_v the specific heat, λ the thermal conductivity, K Taylor–Quinney coefficient, and η the effective shear strain gradient. In comparison with the classical thermoplastic shear instability analysis presented by Bai (1982), the key issue involved in the present scheme is that the strain gradient term is incorporated into the constitutive equation. Hence, the effect of the strain gradient on adiabatic shear banding can be investigated.

3.2. Linear stability analysis

We examine the effect of the strain gradient on the onset of adiabatic shear instability of MMCp characterized by Eqs. (8)–(10). To this end, the linear perturbation method is used for this system of governing equations. Following Bai (1982), we impose a perturbation $(\gamma', \tau', \theta')$ on the smoothly developing homogeneous state $(\gamma_0, \tau_0, \theta_0)$, which is a solution of Eqs. (8)–(10), such that

$$\{\gamma, \tau, \theta\} = \{\gamma_0 + \gamma', \tau_0 + \tau', \theta_0 + \theta'\} \tag{11}$$

$$\{\gamma', \tau', \theta'\} = \{\gamma_*, \tau_*, \theta_*\} \mathrm{e}^{\alpha t + \mathrm{i}ky} \tag{12}$$

and assume that $(\gamma_0, \tau_0, \theta_0)$ vary very slowly with time as compared to $(\gamma', \tau', \theta')$. Whereas $(\gamma', \tau', \theta')$ are the fluctuation quantities departing from the uniform state, and $(\gamma_*, \tau_*, \theta_*)$ are the magnitudes of the perturbation, α is the rate of growth and k is the wave number. It is well known that the onset of adiabatic shear instability is determined by the sign of the real part of α (Bai, 1982; Zhu et al., 1995).

Substituting Eqs. (11) and (12) into Eqs. (9) and (10) and differentiating the constitutive equation (8) leads to

$$\left.\begin{array}{l} [\rho\alpha^2 + (Q_0 + R_0\alpha + \mathrm{i}kS_0)k^2]\gamma_* - P_0k^2\theta_* = 0 \\ [K\tau_0\alpha + K\dot{\gamma}_0(Q_0 + R_0\alpha + \mathrm{i}kS_0)]\gamma_* - [K\dot{\gamma}_0P_0 + \rho c_v\alpha + \lambda k^2]\theta_* = 0 \end{array}\right\} \tag{13}$$

where

$$\left.\begin{array}{ll} Q_0 = \left(\dfrac{\partial\tau}{\partial\gamma}\right)_0 & R_0 = \left(\dfrac{\partial\tau}{\partial\dot{\gamma}}\right)_0 \\ P_0 = -\left(\dfrac{\partial\tau}{\partial\theta}\right)_0 & S_0 = \left(\dfrac{\partial\tau}{\partial\eta}\right)_0 \end{array}\right\} \tag{14}$$

The condition that the determinant of the coefficients of Eq. (13) should be equal to zero leads to the following characteristic equation:

$$\tilde{\alpha}^3 + [C + (1 + A)\tilde{k}^2]\tilde{\alpha}^2 + [A\tilde{k}^2 + 1 - B + D]\tilde{k}^2\tilde{\alpha} + (1 + D)\tilde{k}^4 = 0 \tag{15}$$

where the dimensionless variables are defined as

$$\left.\begin{array}{ll} \tilde{\alpha} = \dfrac{\lambda\alpha}{c_vQ_0} & \tilde{k}^2 = \dfrac{\lambda^2k^2}{\rho c_v^2Q_0} \\ A = \dfrac{c_vR_0}{\lambda} & B = \dfrac{K\tau_0P_0}{\rho c_vQ_0} \\ C = \dfrac{K\lambda P_0\dot{\gamma}_0}{\rho c_vQ_0} & D = \dfrac{\mathrm{i}kS_0}{Q_0} \end{array}\right\} \tag{16}$$

It is clearly seen from Eq. (15), that if the strain gradient effect is neglected, i.e. $D = 0$, the problem is reduced to the strain gradient-independent thermoplastic shearing investigated by Bai (1982) and the instability condition $B > 1$ is derived.

For the present strain gradient-dependent case, first, let us discuss the two extreme situations:

(i) For long wavelength ($k \to 0$), the solutions of the characteristic equation (15) are

$$\left.\begin{aligned} \alpha &= 0 \\ \alpha &= -\frac{KP_0\dot{\gamma}_0}{\rho c_v} \end{aligned}\right\} \tag{17}$$

For this case, shear deformation is stable.

(ii) For short wavelength ($k \to \infty$), the real part of the solution is

$$\mathrm{Re}(\alpha) = -\frac{Q_0}{R_0} \tag{18}$$

Obviously, $\mathrm{Re}(\alpha) < 0$, shear deformation is again always stable. However, there is a negative term $-(B-D)\tilde{k}\tilde{\alpha}^2$ in the spectral equation (15), the instability may occur at a specific set of wave numbers or wavelengths. It is noted that the root of Eq. (15) with the largest positive real part will govern the instability of the homogeneous solution, and is hereafter referred to as the dominant instability mode. For a fixed strain gradient η, the real parts of the roots of Eq. (15) are functions of the wave number. To seek the dominant instability mode, the wave number for which the corresponding $\mathrm{Re}(\alpha) > 0$ is maximum is needed to be determined first. This can be solved by numerical calculations according to the given constitutive equation of MMCp.

As an example, the SiCp/2024 Al matrix composites investigated in the present study is used as a model material. SiCp particles remain elastic in the course of deformation, while 2024 aluminum matrix is assumed to be a strain gradient-independent thermoviscoplastic material. According to our present experimental results and the suggestion made by Li and Jones (1999), the constitutive behavior of 2024 aluminum matrix can be characterized by the following Johnson–Cook type constitutive equation:

$$\tau_{\mathrm{m}} = \left(1 - \frac{\theta - \theta_{\mathrm{r}}}{\theta_{\mathrm{m}} - \theta_{\mathrm{r}}}\right)\left(\frac{\sigma_{\mathrm{m0}}}{\sqrt{3}} + \frac{E_{\mathrm{h}}}{3}\gamma\right)\left(1 + \left(\frac{\dot{\gamma}}{\sqrt{3}D_0}\right)^{1/p}\right) \tag{19}$$

According to Eq. (4), the *strain gradient-dependent* thermoviscoplastic constitutive equation for MMCp can be written as

$$\tau = \left(1 - \frac{\theta - \theta_{\mathrm{r}}}{\theta_{\mathrm{m}} - \theta_{\mathrm{r}}}\right)\left(\frac{\sigma_{\mathrm{m0}}}{\sqrt{3}} + \frac{E_{\mathrm{h}}}{3}\gamma\right)\left(1 + \left(\frac{\dot{\gamma}}{\sqrt{3}D_0}\right)^{1/p}\right)(1 + \hat{l}\eta)^{v} \tag{20}$$

where σ_{m0} is the uniaxial tensile yield stress, and E_{h} is the plastic strain hardening modulus which can be obtained by fitting the experimental result of the matrix. Data of the material to be used in numerical calculation are: $\sigma_{\mathrm{m0}} = 255$ MPa, $E_{\mathrm{h}} = 145.2$ MPa, $D_0 = 6500$ 1/s, $\theta_{\mathrm{m}} = 638$ °C, $\theta_{\mathrm{r}} = 20$ °C, $\rho = 2800$ kg/m^3, $c_v = 921$ J/kg K, $\lambda = 121$ W/m K, $p = 4$, $v = 0.56$. The verification of Eqs. (19) and (20) was shown in Fig. 5. In our numerical analysis, the nominal shear strain rate $\dot{\gamma}_0 = 2000$ 1/s was used. As was discussed previously, we need to seek the wave numbers governing the largest real part of the root of Eq. (15). Fig. 7 presents the typical variations of $\mathrm{Re}(\alpha)$ with wave numbers for three levels of strain gradients. It is seen from Fig. 7 that there exists a specific wave number for which the corresponding $\mathrm{Re}(\alpha)$ takes a peak value.

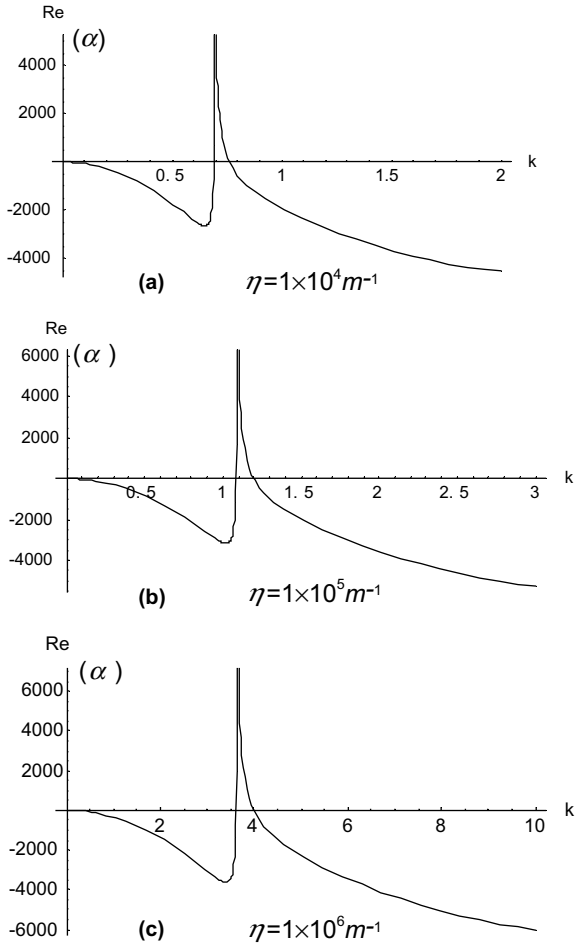

Fig. 7. Variations of the real part of the root of the spectral equation $\mathrm{Re}(\alpha)$ with the wave number k: (a) $\eta = 1 \times 10^4$ m^{-1}; (b) $\eta = 1 \times 10^5$ m^{-1}; (c) $\eta = 1 \times 10^6$ m^{-1}.

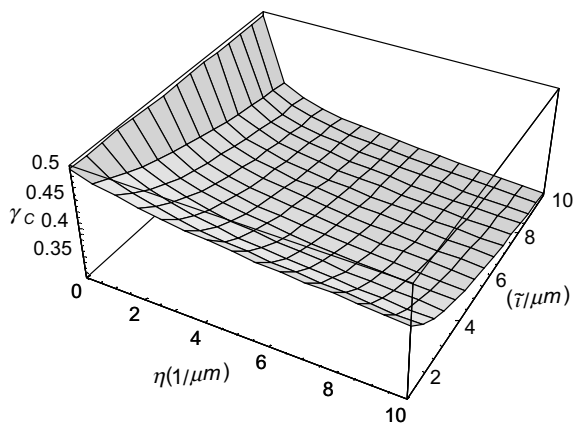

Fig. 8. Variations of the critical shear strain γ_c with the strain gradient η and characteristic length scale $\hat{l}$.

Then, this specific wave number is incorporated into the characteristic equation (15) and the critical instability strain can be calculated for the given strain gradient and characteristic length scale. Changing the values of the strain gradient and the characteristic length scale and repeating the aforementioned calculating process, the effects of the strain gradient η and the characteristic microstructure length scale $\hat{l}$ on the critical instability shear strain γ_c can be investigated. The calculated results are shown in Fig. 8. One can see from Fig. 8 that the critical shear strain for the *strain gradient-independent* 2024 aluminum matrix material is 0.50, which is very close to the experimental value, 0.52. As discussed above, incorporating the reinforcing particles into the metal matrix will induce an inhomogeneous plastic deformation which is characterized by the strain gradient, and the smaller the particle size is the higher the strain gradient is in the material. From Fig. 8, one can furthermore find that the critical shear strain decreases as the strain gradient increases. This means that the strain gradient provides a driving force for the onset of adiabatic shear instability in a two-phase MMCp. Apparently, this analytical result is in accordance with the aforementioned experimental observations.

Now, let us discuss the role of the strain gradient in the formation of adiabatic shear banding in strain gradient-dependent thermoviscoplastic MMCp. In the continuum mechanics viewpoint, it is well known, for the usual gradient-independent thermoplastic adiabatic shear banding, the onset of the instability is the outcome of the competition among the strain hardening, the strain rate hardening, and the thermal softening. For the strain gradient-dependent MMCp, the strain gradient joins the competition. Both the experimental observation and the analytical result demonstrate that high strain gradient will promote the onset of adiabatic shear instability in MMCp reinforced with small particles ($d_p < 10$ μm). The reason is that the composite with small particles is of higher flow stress than that for the large particle composite and its dissipated plastic work is thereby greater than the large particle cases. This, in turn, causes a rapid increase in temperature and produces thermal softening and promotes the onset of adiabatic shear banding. In a dislocation dynamics viewpoint, Hirth and co-workers (Hirth, 1992; Kamat et al., 1991) proposed the model of discontinuous tilt wall of edge dislocations, and predicted the effective stress to drive the formation and propagation of shear band in MMCp. They found that the driving shear stress is inversely proportional to the particle spacing. Whereas the average edge–edge spacing between particles in the MMCp with small particles is smaller than that in MMCp with large particles if the volume fraction of the reinforcing particle is kept fixed (Kamat et al., 1991, Dai et al., 1999). This means that the driving force for the formation and propagation of shear band in MMCp with small particles is higher than that in MMCp with large particles. Obviously, both viewpoints predict an identical role of reinforcing particles in the formation of shear banding in MMCp.

According to the aforementioned discussions, we, therefore, conclude that small reinforcement particles play a two-fold role in the deformation behavior of MMCp: strengthening flow stress and promoting the onset of adiabatic shear banding. So, as an important engineering material, choosing a suitable size of particles as the reinforcement is a key issue for the manufacture and the application of MMCp to high speed deformation.

4. Conclusions

In this paper, the effect of the reinforcing particle size on the formation of adiabatic shear banding in MMCp was investigated using a single-pulse Hopkinson torsion bar (SSHTB) and the linear stability analysis was also made to capture the size-dependent adiabatic shear banding behavior. The results demonstrate that the onset of the adiabatic shear banding depends strongly on the particle size and adiabatic shear band can be readily found in the composite reinforced with small particles. The analysis shows that this size-dependence behavior can be characterized by the strain gradient effect, and the high strain gradient provides a strong driving force for the formation of adiabatic shear banding in MMCp.

Acknowledgements

The authors gratefully acknowledge the financial support of this work by the National Natural Science Fund of China (No.10232040).

References

Aifantis, E.C., 1984. On the microstructure origin of certain inelastic models. Journal of Materials Engineering and Technology ASME 106, 326–330.

Aifantis, E.C., 1992. On the role of gradients on the localization of deformation and fracture. International Journal of Engineering Science 30, 1279–1299.

Aifantis, E.C., 1999. Gradient deformation models at nano, micro, and macroscales. Journal of Materials Engineering and Technology ASME 121, 189–202.

Anand, L., Kim, K.H., Shawki, T.G., 1987. Onset of shear localization in viscoplastic solids. Journal of Mechanics and Physics of Solids 35, 407–429.

Ashby, M.F., 1970. The deformation of plastically non-homogeneous alloys. Philosophical Magazine 21, 399–424.

Bai, Y.L., 1981. A criterion for thermo-plastic shear instability. In: Meyers, M.A., Murr, L.E. (Eds.), Shock Waves and High Strain Rate Phenomena in Metals. Plenum Press, New York, pp. 277–284.

Bai, Y.L., 1982. Thermo-plasticity instability in simple shear. Journal of Mechanics and Physics of Solids 30, 195–207.

Bai, Y.L., Dodd, B., 1992. Adiabatic Shear Localization. Pergamon Press, Oxford.

Batra, R.C., 1987. The initiation and growth of, and interaction among adiabatic shear bands in simple and dipolar materials. International Journal of Plasticity 3, 75–89.

Batra, R.C., Kim, C.H., 1990. Adiabatic shear banding in elastic–viscoplastic nonpolar and dipolar materials. International Journal of Plasticity 6, 127–141.

Batra, R.C., Chen, L., 1999. Shear band spacing in gradient-dependent thermoviscoplastic materials. Computational Mechanics 23, 8–19.

Burns, T.J., 1985. Approximation linear stability analysis of a model of adiabatic shear band formation. Quarterly Applied Mathematics 43, 65–84.

Clifton, R.J., 1980. Adiabatic shear banding. In: Materials Response to Ultra-High Loading Rates, NMAB-356, National Academy of Sciences, Washington, DC, NMAB-356.

Clifton, R.J., Duffy, J., Hartley, K.A., Shawki, T.G., 1984. On critical conditions for shear band formation at high strain rates. Scripta Metallurgy 18, 443–448.

Dai, L.H., Ling, Z., Bai, Y.L., 1999. A strain gradient strengthening law for particle reinforced metal matrix composites. Scripta Materialia 41, 245–251.

Dai, L.H., Ling, Z., Bai, Y.L., 2000. Strain gradient effect on the initiation of adiabatic shear localization in metal matrix composites. Key Engineering Materials 177–180, 401–406.

Dai, L.H., Ling, Z., Bai, Y.L., 2001. Size-dependent inelastic behavior of particle reinforced metal matrix composites. Composites Science and Technology 61, 1057–1063.

El-Magd, E., 1997. Localization of deformation and damage under adiabatic compression. Journal de Physique III C3, 511–516.

Fleck, N.A., Hutchinson, J.W., 1997. Strain gradient plasticity. Advance in Applied Mechanics 33, 295–361.

Fressengeas, C., Molinari, A., 1987. Instability and Localization of plastic flow in shear at high strain rates. Journal of Mechanics and Physics of Solids 33, 185–211.

Gao, H., Huang, Y., Nix, W.D., Hutchinson, J.W., 1999a. Mechanism-based strain gradient plasticity—I. Theory. Journal of Mechanics and Physics of Solids 47, 1239–1263.

Gao, H., Huang, Y., Nix, W.D., Hutchinson, J.W., 1999b. Modeling plasticity at he micrometer scale. Naturwissenschaften 86, 507–515.

Green, A.E., Mcinnis, B.C., Naghdi, P.M., 1968. Elastic–plastic continua with simple force dipole. International Journal of Engineering Science 6, 373–394.

Hirth, J.P., 1992. A model for a propagation shear band on the basis of tilt wall dislocation array. Applied Mechanics Reviews 45, s71–s74.

Kamat, S.V., Rollett, A.D., Hirth, J.P., 1991. Plastic deformation in Al alloy matrix alumina particulate composites. Scripta Metallurgica et Materialia 25, 27–32.

Lee, S., Cho, K.M., Kim, K.C., Choi, W.B., 1993. Adiabatic shear band formation in Ai–SiCw composites. Metallurgical Transactions 24A, 895–900.

Li, Q.M., Jones, N., 1999. Shear and adiabatic shear failures in an impulsively loaded fully clamped beam. International Journal of Impact Engineering 22, 589–607.
Ling, Z., 2000. Deformation behavior and Microstructure effect in 2124Al/SiCp composite. Journal of Composite Materials 34, 101–115.
Ling, Z., Luo, L., Dodd, B., 1994. Experimental study on the formation of shear bands and effect of microstructure in Al-2124/SiCp composites under dynamic compression. Journal de Physique III 4, 453–458.
Liu, L.F., Dai, L.H., Yang, G.W., 2003. Strain gradient effects on deformation strengthening behavior of particle reinforce metal matrix composites. Materials Science and Engineering A 345, 190–196.
Massey, H.F., 1921. The flow of a metal during forging. In: Proceedings of Manchester Axxoc Engineers, pp. 21–26. Reprinted by the National Machinery Co, Tiffon, OH.
Meyer, L.W., Staskewisch, E., Burblies, A., 1994. Adiabatic shear failure under dynamic compression/shear loading. Mechanics of Materials 17, 203–214.
Meyers, M.A., 1994. Dynamic Behavior of Materials. John Wiley & Sons, New York.
Meyers, M.A., Chawla, K.K., 1983. Mechanical Metallurgy. Prentice Hall Inc, Englewood Cliffs, NJ.
Meyers, M.A., Nesterenko, V.F., LaSalvia, J.C., Xue, Q., 2001. Shear localization in dynamic deformation of materials: microstructural evolution and self-organization. Materials Science and Engineering A 317, 204–225.
Molinari, A., Clifton, R.J., 1987. Analytical characterization of shear localization in thermoviscoplastic solids. Journal of Applied Mechanics ASME 54, 806–812.
Perzyna, P.V., 1998. Localization and Fracture Phenomena in Inelastic Solids. Springer-Verlag, Berlin.
Ramesh, K.T., 1994. On the localization of shearing deformation in tungsten heavy alloys. Mechanics of Materials 17, 165–173.
Rogers, H.C., 1979. Adiabatic plastic deformation. Annual Review of Materials 9, 283–311.
Schoenfeld, S.E., Wright, T.W., 2003. A failure criterion based on material instability. International Journal of Solids and Structures 40, 3021–3037.
Shawki, T.G., Clifton, R.J., 1989. Shear band formation in thermal viscoplastic materials. Mechanics of Materials 8, 13–43.
Shawki, T.G., 1992. The phenomenon of shear strain localization in dynamic viscoplasticity. Applied Mechanics Review 45, 46–61.
Sluys, L.J., Estrin, Y., 2000. The analysis of shear banding with a dislocation based gradient plasticity model. International Journal of Solids and Structures 37, 7123–7142.
Sluys, L.J., de Borst, R., Muhlhaus, H.B., 1993. Wave propagation, localization and dispersion in a gradient-dependent medium. International Journal of Solids and Structures 30, 1153–1171.
Tresca, H., 1878. On further applications of the flow solids. Proceedings of the Institute of Mechanical Engineers 30, 301–345.
Wright, T.W., Ockendon, H., 1996. A scaling law for the effect of inertia on the formation of adiabatic shear bands. International Journal of Plasticity 12, 927–934.
Wright, T.W., 2002. The Physics and Mathematics of Adiabatic shear bands. Cambridge University Press, Cambridge.
Wright, T.W., 2003. On the speed of an unconstrained shear band in a perfectly plastic material. International Journal of Solids and Structures 40, 871–879.
Xue, Q., Shen, L.T., Bai, Y.L., 1995a. A modified split Hopkinson torsional bar in studying shear localization. Measurement Science and Technology 6, 1557–1565.
Xue, Q., Shen, L.T., Bai, Y.L., 1995b. Elimination of loading reverberation in the split Hopkinson torsional bar. Review Scientific Instrument 66, 5298–5304.
Xue, Q., Meyers, M.A., Nesterenko, V.F., 2002. Self-organization of shear bands in titanium and Ti–6Al–4V alloy. Acta Materialia 50, 575–595.
Zbib, H.M., Aifantis, E.C., 1992. On the gradient-dependent theory of plasticity and shear banding. Acta Mechanica 92, 209–225.
Zener, C., Hollomon, J.H., 1944. Effect of strain rate upon plastic flow of steel. Journal of Applied Physics 15, 22–32.
Zhou, M., 1998a. The growth of shear bands in composite microstructures. International Journal of Plasticity 14, 733–754.
Zhou, M., 1998b. Effects of microstructure on resistance to shear localization for a class of metal matrix composites. Fatigue and Fracture of Engineering Materials and Structures 21, 425–438.
Zhu, H.T., Zbib, H.M., Aifantis, E.C., 1995. On the role of strain gradients in adiabatic shear banding. Acta Mechanica 111, 111–124.